(Preprint) AAS 15-738

UNCUED SATELLITE INITIAL ORBIT DETERMINATION USING SIGNALS OF OPPORTUNITY

Johnny L. Worthy III[*], Marcus J. Holzinger[†]

This paper investigates the application of signal of opportunity based multilateration to generate initial orbit estimates. Using at least 4 observer stations, the time differential of arrival of signals of opportunity can be measured and used to determine a 3D position estimate of the source of the signal with some associated covariance on the position estimate. While this solution gives the position of the object, admissible region theory may be applied to bound the possible velocity states belonging to a particular source. Two constraints are considered and analytically derived for the time differential of arrival problem to constraint the possible velocity solutions for a given position estimate. Once a joint admissible region is formed from these constraints, it may be sampled and used as an initial distribution for a particle filter. This work shows an example application of particle filter initiation with a time differential of arrival measurement based admissible region.

INTRODUCTION

Multilateration is a general navigation technique that uses a measurement of the difference between stations that broadcast or receive a signal. This measurement is of the difference in the time of arrival of the signals often referred to as time differential of arrival (TDoA). Multilateration solves the problem of locating a receiver with a network of transmitters or locating a transmitter with a network of receivers. Measuring TDoA at the receiver locations generates range information as the signals travel at the speed of light and the position of the receivers is already known. Thus the solution for finding a transmitter with two receivers lies on a hyperboloid [1]. The addition of more receiving devices generates additional hyperboloids and geometrically the emitter must be located at the intersection of the hyperboloids. In contrast with GPS, multilateration with TDoA does not require synchronized clocks nor does it require knowledge of the time of origin of the signal. This enables passive geolocation and it has been implemented in aircraft for operation similar to ADS-B and SSR [2] [3]. Further, with the ubiquity of communications signals emitted from a variety of known sources, the concept of passive geolocation is of recent interest for Earth-based location and navigation systems because GNSS signals can be jammed and interrupted [4]. These so-called signals of opportunity present possible robust and persistent navigation capabilities with existing systems. In general, the applications of TDoA focus on geolocating targets on the surface of the Earth. However, the techniques apply to satellites and space objects as well and TDoA provides an alternative phenomenology for observing the state of a space object.

TDoA techniques for space applications were introduced by Escobal et. al. in the 1970s [5]. This work demonstrates a laser ranging network capable of one centimeter accuracies in determining

[*]Graduate Researcher, School of Aerospace Engineering, Georgia Institute of Technology
[†]Assistant Professor, School of Aerospace Engineering, Georgia Institute of Technology.

the position of a vehicle passing over the ranging network [5]. However, since such a network did not exist, Escobal went on to show that a network of ground stations receiving signals are capable of providing range information. In this work, Escobal et. al. introduces a multilateration method for a spacecraft (or airplane) passing over a network of at least five ground station by using TDoA measurements [6]. An actual solution to the geolocation problem considered by Escobal et. al. is first presented in [7]. Ho et. al. defines the geolocation problem applied to a transmitter on the Earth's surfaces being located by a set of geostationary satellite receivers. By restricting the location problem to objects on the surface of the Earth, the geolocation solution is simplified since the solution must lie on the Earth and a minimum of three receivers is required, but if the altitude of the transmitter is unknown at least four receivers are required. An exact solution for the both cases is given in [7]. This work is the basis of much of the research done in this area. Ho et. al. incorporated frequency difference of arrival (FDoA) in to the solution by accounting for the relative movement of the sensors and the effect of the frequency shift due to the motion [8]. Fletcher and Okello demonstrate that by utilizing moving targets, only two receivers are needed by incorporating multiple TDoA measurements [9] [10]. Mušicky et. al. detail geolocation using TDoA as well as frequency difference of arrival (FDoA) [11] by using them as arguments to the Complex Ambiguity Function (CAF) [12].

General application of TDoA localization for satellites or other space objects is largely absent in the literature. The advantages of such a system lie in the potential use of signals of opportunity as the signals received by the ground station. These signals could then be used identically to typical beacons used for geolocation via TDoA. To demonstrate the feasibility of TDoA for space objects with Earth based receiving stations, this paper 1) states the TDoA problem and assesses the contribution of observer error to the TDoA solution accuracy, 2) derives the TDoA problem as an admissible region problem, 3) redresses orbit energy and periapse radius constraints for the TDoA admissible region in inertial cartesian coordinates, and 4) simulates the initialization of a particle filter from TDoA observation system.

TIME DIFFERENTIAL OF ARRIVAL SOLUTION

The basic problem geometry for time differential ranging problems is shown in Figure 1. The receiver positions are denoted as $\mathbf{r}_{s,i}$ and are assumed to be known. The position of the source of the signal is denoted as $\mathbf{r}$ and is the desired quantity. Each of the ranges ρ_i is determined by knowledge of the time it takes a signal to propagate from the source to each of the i receivers. From the basic problem geometry, the following system of equations can be solved to give a position estimate of the source

$$\rho_1 = c\Delta t_1 = \|\mathbf{r}_{s,1} - \mathbf{r}\| \tag{1}$$

$$\rho_2 = c\Delta t_2 = \|\mathbf{r}_{s,2} - \mathbf{r}\| \tag{2}$$

$$\rho_3 = c\Delta t_3 = \|\mathbf{r}_{s,3} - \mathbf{r}\| \tag{3}$$

where c is the propagation speed of the signal and Δt_i represents the time it takes the signal to travel from the source to the i^{th} observer. The general method of determining $\mathbf{r}$ using hyperbolic localization is introduced by Chan and Ho [13]. The actual time difference Δt_i giving range ρ_i may not generally be measured unless the clocks at the receiver and the source are synchronized. For TDoA measurements synchronized clocks are not utilized and thus a relative formulation of Eqns. (1)-(3) is necessary. Figure 1 shows this relative formulation where Observer i receives the signal first with some unknown differential τ. Then Observer j receives the signal with a delay relative

to Observer i of $\Delta t_{i,j}$. Many variations and applications of this approach have been introduced [8] [14] [9] [10] [11] [15]. In the relative formulation, one of the receivers acts as a reference once the signal is detected. The difference in time between the arrival at the reference and each of the other receivers comprises the measurements. An integral part of this process is the identification of the signal at the reference and the subsequent identification of the signal by the the observers. Matched filters are frequently used with TDoA systems to determine the signal arrival time and/or extract the unknown signals at the reciever [16] [17] [18] [19]. Future work will include a full discussion and application of such filters to simulate a TDoA observation system for analysis.

In TDoA systems, the true range ρ_i can then be expressed as a function of a pseudorange p_i and a delay τ, where pseudorange is defined as

$$p_i = c\Delta t_{1,i}$$

where c is the speed of light, and $\Delta t_{1,i}$ is the time difference of arrival of the signal relative to receiver 1. Since, the first receiver is taken as the reference $p_1 = 0$. Now Eqns. (1)-(3) may be rewritten as a system of 4 equations where τ is an unknown in addition to the source location.

$$c\tau = \|\mathbf{r}_{s,1} - \mathbf{r}\| \tag{4}$$
$$p_2 + c\tau = \|\mathbf{r}_{s,2} - \mathbf{r}\| \tag{5}$$
$$p_3 + c\tau = \|\mathbf{r}_{s,3} - \mathbf{r}\| \tag{6}$$
$$p_4 + c\tau = \|\mathbf{r}_{s,4} - \mathbf{r}\| \tag{7}$$

The measurement function for this observation may then be written as

$$\mathbf{y} = \mathbf{h}(\mathbf{r}, \mathbf{r}_{s,i}, \tau) = \frac{1}{c}\left[\|\mathbf{r}_{s,i} - \mathbf{r}\| - c\tau\right] \tag{8}$$

which physically signifies the time differential of arrival of the signal between locations i and j. With this form, four receivers are required to obtain an estimate of the position of the source of the signal. Note, in this paper, all positions and velocities are expressed in the Earth centered inertial frame.

Uncertainties in TDoA Measurements

Eqns. (4)-(7) are very sensitive to timing accuracy as well as the position knowledge of the receivers. Thus it is of interest to be able to quantify how the timing and observer position errors and uncertainties affect the accuracy of the position estimate. Treating Eqns. (4)-(7) as a vector valued function and equating to zero as follows

$$\mathbf{e}(\mathbf{r}, \mathbf{y}, \mathbf{k}) = c(\mathbf{y}_{\text{meas}} - \mathbf{y}) = c(\mathbf{y}_{\text{meas}} - \mathbf{h}(\mathbf{r}, \mathbf{r}_{s,i}, \tau)) \tag{9}$$
$$= \begin{bmatrix} c\tau - \|\mathbf{r}_{s,1} - \mathbf{r}\| \\ p_2 + c\tau - \|\mathbf{r}_{s,2} - \mathbf{r}\| \\ p_3 + c\tau - \|\mathbf{r}_{s,3} - \mathbf{r}\| \\ p_4 + c\tau - \|\mathbf{r}_{s,4} - \mathbf{r}\| \end{bmatrix} = \mathbf{0} \tag{10}$$

where $\mathbf{y} \in \mathbb{R}^4$ is the measurement vector and $\mathbf{k} \in \mathbb{R}^{12}$ is a parameter vector containing the positions of the observer. The measurement vector may be written as

$$\mathbf{y} = \begin{bmatrix} \Delta t_{1,1} & \Delta t_{1,2} & \Delta t_{1,3} & \Delta t_{1,4} \end{bmatrix}^T \tag{11}$$

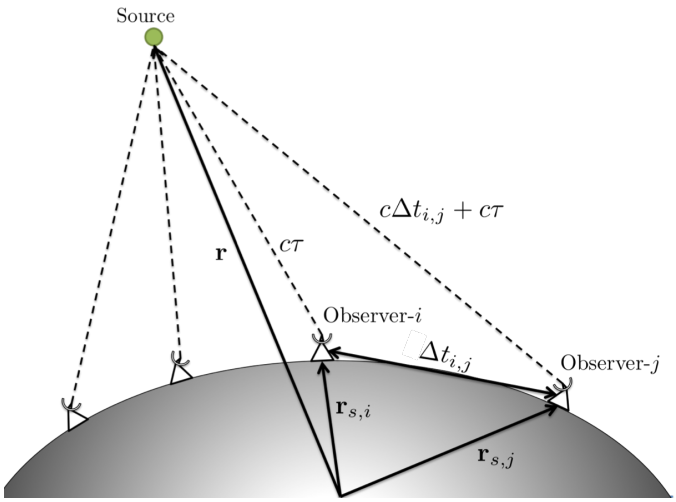

Figure 1: The geometry of the TDoA problem in the Earth centered inertial frame. $\Delta t_{i,j}$ represents the time difference between the signal arriving at observer i and j.

and the parameter vector may be written as

$$\mathbf{k} = \begin{bmatrix} \mathbf{r}_{s,1}^T & \mathbf{r}_{s,2}^T & \mathbf{r}_{s,3}^T & \mathbf{r}_{s,4}^T \end{bmatrix}^T \tag{12}$$

A first order Taylor series approximation is used to define a covariance on the position estimate based on covariances of the timing accuracy and observer position knowledge. The first order Taylor series is given by

$$\mathbf{e}(\mathbf{r} + \delta\mathbf{r}, \mathbf{y} + \delta\mathbf{y}, \mathbf{k} + \delta\mathbf{k}) \approx \mathbf{e}(\mathbf{r}, \mathbf{y}, \mathbf{k}) + \frac{\partial \mathbf{e}}{\partial \mathbf{r}}\delta\mathbf{r} + \frac{\partial \mathbf{e}}{\partial \mathbf{y}}\delta\mathbf{y} + \frac{\partial \mathbf{e}}{\partial \mathbf{k}}\delta\mathbf{k} \tag{13}$$

which can be rewritten as

$$-\frac{\partial \mathbf{e}}{\partial \mathbf{r}}\delta\mathbf{r} = \frac{\partial \mathbf{e}}{\partial \mathbf{y}}\delta\mathbf{y} + \frac{\partial \mathbf{e}}{\partial \mathbf{k}}\delta\mathbf{k} \tag{14}$$

The matrix $\partial\mathbf{e}/\partial\mathbf{r} \in \mathbb{R}^{4\times4}$ is a full rank, and thus invertible, matrix and Eqn. (14) can be rewritten as

$$\delta\mathbf{r} = -\left[\frac{\partial \mathbf{e}}{\partial \mathbf{r}}^{-1}\right]\begin{bmatrix}\frac{\partial \mathbf{e}}{\partial \mathbf{y}} & \frac{\partial \mathbf{e}}{\partial \mathbf{k}}\end{bmatrix}\begin{bmatrix}\delta\mathbf{y} \\ \delta\mathbf{k}\end{bmatrix} \tag{15}$$

Combining the measurement and parameter vectors into a single vector $\delta\mathbf{z}$. If the covariances on the errors for $\mathbf{z}$ is known, then $\delta\mathbf{z}$ may be treated as a random variable $\delta\mathbf{Z} \sim \mathcal{N}(\mathbf{0}, \mathbf{P}_z)$ and Eqn. (15) may be written stochastically as

$$\delta\mathbf{R} = \frac{\partial \mathbf{e}}{\partial \mathbf{r}}^{-1}\frac{\partial \mathbf{e}}{\partial \mathbf{z}}\delta\mathbf{Z} \tag{16}$$

where $\mathbf{R}$ is now a random variable. Defining,

$$\mathbf{M} = \frac{\partial \mathbf{e}}{\partial \mathbf{r}}^{-1}\frac{\partial \mathbf{e}}{\partial \mathbf{z}} \tag{17}$$

he statistics of $\delta\mathbf{R}$ are determined as follows.

$$\mathbb{E}[\delta\mathbf{R}] = \mathbb{E}[\mathbf{M}\delta\mathbf{Z}] \tag{18}$$

$$= \mathbf{M}\mathbb{E}[\delta\mathbf{Z}] = \mathbf{0} \tag{19}$$

The covariance of $\delta\mathbf{R}$ is determined similarly, yielding

$$\mathbf{P_r} = \mathbf{M}\mathbf{P}_z\mathbf{M}^T \tag{20}$$

Eqn. (20) gives the covariance on the estimate $\mathbf{r}$ for a TDoA system based on timing inaccuracies and observer position knowledge error.

Dilution of Precision

The geometry presented in Figure 1 also plays an integral role in the accuracy of the overall solution. For GPS, the geometry of the satellite receivers is important to the overall accuracy of the GPS position estimate. For TDoA, the accuracy of the estimate of the position of the source changes based on $\mathbf{r}$ itself. To quantify this, it is possible to define an equivalent dilution of precision (DOP) metric which informs the accuracy of the TDoA position estimate [20] [21]. Consider the gradient matrix $\mathbf{H}$ defined as the partial derivative of the measurements $\mathbf{y}$ with respect to $\mathbf{r}$,

$$\mathbf{H} = \frac{\partial \mathbf{y}}{\partial \mathbf{r}} \tag{21}$$

The $\mathbf{H}$ matrix is representative of how sensitive the measurements are to the position. Following the approach outlined in [20], the dilution of precession for the TDoA problem is defined as

$$D_P = \sqrt{\mathrm{tr}\left((\mathbf{H}^{\mathrm{T}}\mathbf{P}_{\mathrm{t}}^{-1}\mathbf{H})^{-1}\right)} \tag{22}$$

where $\mathbf{P}_t$ is the covariance of the measurement timing error in meters. The quantity D_P is unitless and relates the timing uncertainty (in meters) to the overall position estimate uncertainty [20]. It signifies that with some timing uncertainty expressed in meters by $c\sigma_t$, the overall position uncertainty in the estimate is given by $c\sigma_t D_P$. As such, it is desired that $D_P < 1$, which implies that the accuracy of the estimated position $\mathbf{r}$ is only significantly affected by the timing accuracy of the sensors.

ADMISSIBLE REGION FOR TDOA MEASUREMENTS

The TDoA solution only gives the position of the source object. An admissible region approach may then be used to constrain the possible source velocity solutions. Note that it is possible to get a full state estimate if several TDoA observations are made, but since this approach is based on TDoA using signals of opportunity, it is unlikely that more than one observation will be captured over a short time period. The admissible region approach is well defined in the literature [22], [23], [24],[25], [26].

Deriving the Admissible Region

An admissible region problem formulation of the TDoA problem can be derived by applying the process outlined in [27] which is founded on the process shown in [28] for radar observations. The state vector of interest is the cartesian state of the source object given by

$$\mathbf{x}^T = \begin{bmatrix}\mathbf{r}^T & \mathbf{v}^T\end{bmatrix} \tag{23}$$

where $\mathbf{r}$, as already defined, is the position of the source obtained by solving Eqns. (4)-(7) and $\mathbf{x}_u$ is the velocity of the source object. It is clear from Eqn. (9) that the determined state is the position of the source $\mathbf{r}$ and the undetermined state is the velocity of the source $\mathbf{x}_u$, allowing,

$$\mathbf{x}^T = \begin{bmatrix} \mathbf{x}_d^T & \mathbf{x}_u^T \end{bmatrix} \tag{24}$$

Thus, the state vector may be partitioned and Eqn. (9) may be rewritten as

$$\mathbf{e}(\mathbf{x}_d, \mathbf{x}_u, \mathbf{y}, \mathbf{k}) = \begin{bmatrix} c\tau - \|\mathbf{r}_{s,1} - \mathbf{x}_d\| \\ p_2 + c\tau - \|\mathbf{r}_{s,2} - \mathbf{x}_d\| \\ p_3 + c\tau - \|\mathbf{r}_{s,3} - \mathbf{x}_d\| \\ p_4 + c\tau - \|\mathbf{r}_{s,4} - \mathbf{x}_d\| \end{bmatrix} = \mathbf{0} \tag{25}$$

where $\mathbf{x}_u$ belongs a continuum of source velocities yielding the same position estimate.

A set of hypothesis constraints may be constructed for the TDoA problem to bound this continuum of possible solutions. These constraints are written in the form

$$\kappa_i(\mathbf{x}_d, \mathbf{x}_u; \mathbf{k}, t) \leq 0 \tag{26}$$

where κ_i is a scalar valued function representing the i^{th} constraint. The admissible region $\mathcal{AR}_i$ for the i^{th} TDoA constraint is defined as

$$\mathcal{AR}_i := \{\mathbf{x}_u \in \mathbb{R}^3 \,|\, \kappa_i(\mathbf{x}_d, \mathbf{x}_u; \mathbf{k}, t) \leq 0\} \tag{27}$$

For a given TDoA constraint, $\mathcal{AR}_i$ is a 3-dimensional region over the velocity space of the source object. The total admissible region $\mathcal{AR}$ is given by

$$\mathcal{AR} = \mathcal{AR}_1 \cap \mathcal{AR}_2 \cap \cdots \cap \mathcal{AR}_c \tag{28}$$

where c is the total number of constraint hypothesis applied.

Constraints for TDoA

The constraint hypotheses for a TDoA $\mathcal{AR}$ are functions of the velocity of the source. The two constraints considered are on the orbital energy and the radius of periapsis of the orbit. These constraints are derived in topocentric spherical coordinates in [28] and will be derived in inertial cartesian coordinates in this section.

The primary constraint for observing Earth objects ensures that the object is in a closed orbit. Rearranging the vis-viva equation for a Keplerian orbit gives

$$\|\mathbf{x}_u\| = \mu \left(\frac{2}{\mathbf{x}_d} - \frac{1}{a} \right) \tag{29}$$

Using Eqn. (29), a constraint on the maximum velocity of the source is derived by allowing $a \to \infty$ yielding

$$\|\mathbf{x}_u\| - \mu \left(\frac{2}{\|\mathbf{x}_d\|} \right) \leq 0 \tag{30}$$

where states satisfying Eqn. (30) are in closed orbits. Eqn. (30) can be rewritten in constraint form as

$$\kappa_1(\mathbf{x}_d, \mathbf{x}_u, \mathbf{k}, t) = \|\mathbf{x}_u\| - \mu\left(\frac{2}{\|\mathbf{x}_d\|}\right) \tag{31}$$

It is also important to exclude velocities which do not generate a sustainable orbit, thus imposing a minimum periapse radius to ensure the source object does not enter the Earth's atmosphere. The periapse radius of an orbit is given by

$$r_p = a(1-e) \tag{32}$$

where r_p is the periapse radius, a is the semi-major axis, and e is the eccentricity of the orbit. The eccentricity is a function of the specific orbital energy, ε, and the specific angular momentum $\mathbf{h}$ given by

$$e = \sqrt{1 + \frac{2\varepsilon h^2}{\mu^2}} \tag{33}$$

At periapsis, the specific angular momentum is given simply by $h = \|\mathbf{x}_d\|\|\mathbf{x}_u\|\cos\gamma$. The specific orbital energy may be expressed as

$$\varepsilon = \frac{\|\mathbf{x}_u\|^2}{2} - \frac{\mu}{\|\mathbf{x}_d\|} \tag{34}$$

Because the geometry is simply a sphere, a representative admissible region of the energy constraint will not be shown.

Combining Eqns. (32), (33), (34), the minimum periapse radius constraint can be written as

$$r_{p,\min} + \frac{\mu\left(\sqrt{1 - \frac{r^2 v^2 \cos^2\gamma(\frac{2\mu}{r^2} - v^2)}{\mu^2}} - 1\right)}{\frac{2\mu}{r^2} - v^2} \leq 0 \tag{35}$$

where $r = \|\mathbf{x}_d\|$, $v = \|\mathbf{x}_u\|$, and $r_{p,\min}$ is the minimum allowable periapse radius. For simplicity, define

$$c_1 = \frac{2\mu}{r^2} - v^2 \tag{36}$$

$$c_2 = 1 - \frac{r^2 v^2 \cos^2\gamma(\frac{2\mu}{r^2} - v^2)}{\mu^2} \tag{37}$$

Then Eqn. (53) may be written as

$$c_1 r_{p,\min} + \mu(c_2^{1/2} - 1) \leq 0 \tag{38}$$

After manipulation, Eqn. (38) becomes

$$\mu^2 c_2^2 - \mu^2 + 2r_{p,\min}c_1 - r_{p,\min}^2 c_1^2 \leq 0 \tag{39}$$

Expanding and collecting terms in Eqn. (39) gives a 4^{th} order polynomial in v defining the surface of the admissible region for the periapse radius constraint,

$$0 = (r^2\cos^2\gamma - r_{p,\min}^2)v^4 + (-2\mu r_{p,\min} - 2\mu r\cos^2\gamma + \frac{4\mu r_{p,\min}^2}{r})v^2 + (\frac{4\mu^2 r_{p,\min}}{r} - \frac{4\mu^2 r_{p,\min}^2}{r^2}) \tag{40}$$

Defining $l = v^2$ then an analytical solution for v exists by solving the quadratic formula for l. Multiplying through by r^2 and letting

$$c_3 = (r^4\cos^2\gamma - r^2 r_{p,\min}^2) \tag{41}$$

$$c_4 = (-2r^2\mu r_{p,\min} - 2\mu r^3\cos^2\gamma + 4\mu r^3 r_{p,\min}^2) \tag{42}$$

$$c_5 = (4r\mu^2 r_{p,\min} - 4\mu^2 r_{p,\min}^2) \tag{43}$$

Then,

$$l = \frac{-c_4 \pm \sqrt{c_4^2 - 4c_3c_5}}{2c_3} \tag{44}$$

$$v = \pm\sqrt{l} \tag{45}$$

In general, there are 4 solutions for v, but since $v \geq 0$, conditions on real solutions for can be analytically stated. For a real solution for v, Eqn. (44) must satisfy $l \geq 0$ and $l \in \mathbb{R}$. For $l \in \mathbb{R}$, there are two possible cases which result in a real, positive value for v. The first case is,

$$l_1 = \frac{-c_4 + \sqrt{c_4^2 - 4c_3c_5}}{2c_3} \tag{46}$$

$$= \frac{\sqrt{\mu^2 r^4(r_{p,\min} - r\cos^2\gamma)^2} + 2\mu r r_{p,\min}^2 - \mu r^2 r_{p,\min} - \mu r^3\cos^2\gamma}{r^2 r_{p,\min}^2 - r^4\cos^2\gamma} \tag{47}$$

The second case is,

$$l_2 = \frac{-c_4 - \sqrt{c_4^2 - 4c_3c_5}}{2c_3} \tag{48}$$

$$= -\frac{\sqrt{\mu^2 r^4(r_{p,\min} - r\cos^2\gamma)^2} - 2\mu r r_{p,\min}^2 + \mu r^2 r_{p,\min} + \mu r^3\cos^2\gamma}{r^2 r_{p,\min}^2 - r^4\cos^2\gamma} \tag{49}$$

For real solutions for v it is required that $l_1 \geq 0$ and $l_2 \geq 0$. The square root term in the expression for l_1 and l_2 is always positive, thus for a real $v_1 = +\sqrt{l_1}$ to exist, the following must be satisfied

$$\sqrt{\mu^2 r^4(r_{p,\min} - r\cos^2\gamma)^2} + 2\mu r r_{p,\min}^2 \geq \mu r^2 r_{p,\min} + \mu r^3\cos^2\gamma \tag{50}$$

$$r^2 r_{p,\min}^2 - r^4\cos^2\gamma \geq 0 \tag{51}$$

For a real $v_2 = +\sqrt{l_2}$ to exist,

$$\begin{aligned}\text{sign}(\mathrm{r}^2\mathrm{r}_{\mathrm{p,min}}^2 - \mathrm{r}^4\cos^2\gamma) = -\text{sign}(&\sqrt{\mu^2\mathrm{r}^4(\mathrm{r}_{\mathrm{p,min}} - \mathrm{r}\cos^2\gamma)^2} \\ &- 2\mu r r_{p,\min}^2 + \mu r^2 r_{p,\min} + \mu r^3\cos^2\gamma)\end{aligned} \tag{52}$$

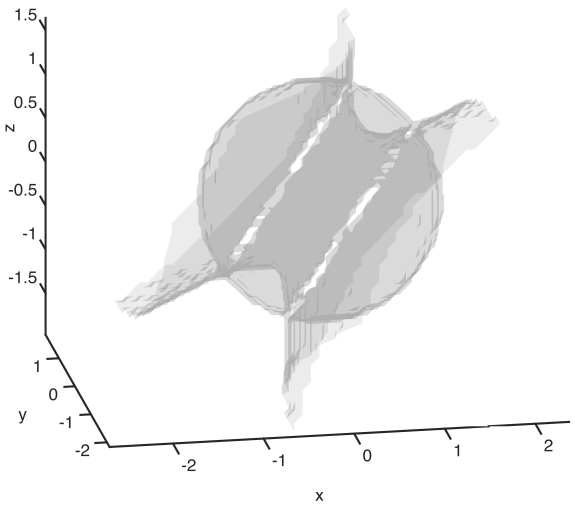

Figure 2: Representative periapse radius constraint boundary

Any negative solutions for l_1 or l_2 will yield imaginary solutions for v_1 or v_2. Solutions for v that are imaginary or negative for a given $r_{p,\min}$, r, and γ are ignored. The admissible region for v then has two cases, either both l_1 and l_2 are real in which case there are two solutions for v given as $v_1 = +\sqrt{l_1}$ and $v_2 = +\sqrt{l_2}$ or only one of l_1 or l_2 is real in which case $v_3 = +\sqrt{l_i}$ where i is the index of the real solution. The geometry for the admissible region of the periapse constraint is essential a sphere, defined since $v_3 = \max(\mathrm{v}_1, \mathrm{v}_2)$. For values of γ yielding v_1 and v_2, valid solutions for v must satisfy $\min(\mathrm{v}_1, \mathrm{v}_2) \leq \mathrm{v} \leq \max(\mathrm{v}_1, \mathrm{v}_2)$. For values of γ yielding v_3, valid solutions must satisfy $v > v_3$. This admissible region constraint is visualized in Figure 2.

In constraint form, the periapse equation may be written as

$$\kappa_2(\mathbf{x}_d, \mathbf{x}_u, \mathbf{k}, t) = c_3 v^4 + c_4 v^2 + c_5 \tag{53}$$

Thus, the total $\mathcal{AR}$ for the TDoA problem considered in this paper is defined as

$$\mathcal{AR} = \{\mathbf{x}_u \in \mathbb{R}^3 | \kappa_1(\mathbf{x}_d, \mathbf{x}_u, \mathbf{k}, t) \leq 0 \cap \kappa_2(\mathbf{x}_d, \mathbf{x}_u, \mathbf{k}, t) \leq 0)\} \tag{54}$$

From Eqn. (54), the probability that a velocity resides in $\mathcal{AR}$ may be written as a piecewise membership function

$$\mathbb{P}(\mathbf{x}_u \in \mathcal{AR}) = \begin{cases} 1 & \kappa_1(\mathbf{x}_d, \mathbf{x}_u, \mathbf{k}, t) \leq 0 \cap \kappa_2(\mathbf{x}_d, \mathbf{x}_u, \mathbf{k}, t) \leq 0 \\ 0 & \text{otherwise} \end{cases} \tag{55}$$

But, since the analytical conditions for $\kappa_1(\mathbf{x}_d, \mathbf{x}_u, \mathbf{k}, t) \leq 0$ and $\kappa_2(\mathbf{x}_d, \mathbf{x}_u, \mathbf{k}, t) \leq 0$ have been defined, Eqn. (55) is simply given by

$$\mathbb{P}(\mathbf{x}_u \in \mathcal{AR}) = \begin{cases} 1 & v \leq \frac{\mu}{2r}, \max(\mathrm{v}_1, \mathrm{v}_2) \leq \mathrm{v} \leq \max(\mathrm{v}_1, \mathrm{v}_2) \\ 0 & \text{otherwise} \end{cases} \tag{56}$$

or

$$\mathbb{P}(\mathbf{x}_u \in \mathcal{AR}) = \begin{cases} 1 & v \leq \frac{\mu}{2r}, v \geq v_3 \\ 0 & \text{otherwise} \end{cases} \tag{57}$$

depending on the number of real, positive solutions to Eqn. (53).

The Effect of Uncertainty

It is previously shown how the observer position and timing errors contribute to the accuracy of the position estimate through Eqn. (20). These uncertainties and errors contribute to how the admissible region is constructed as well. The process outlined in [27] is used to determine the contribution of the uncertainties and errors to $\mathcal{AR}$. Using the same Taylor series approach as shown in Eqn. (11), the first order Taylor series approximation of each constraint is given by

$$-\frac{\partial \kappa_i}{\partial \mathbf{x}_u}\delta\mathbf{x}_u = \frac{\partial \kappa_i}{\partial \mathbf{x}_d}\delta\mathbf{x}_d \tag{58}$$

Each constraint κ_i is a scalar function and the resulting partial derivative $\partial\kappa_i/\partial\mathbf{x}_u$ cannot be inverted. Additional relationships must be derived so that an expression for $\delta\mathbf{x}_u$ can be written. In a process identical to what is outlined in [27], orthogonal vectors can be constructed such that the $\delta\mathbf{x}_u$ is orthogonal to the surface defined by κ_i. For the TDoA admissible region, the first orthogonal vector $\mathbf{t}_1$ can be taken as any vector orthogonal to $\partial\kappa_i/\partial\mathbf{x}_u$ such that $\partial\kappa_i/\partial\mathbf{x}_u \cdot \mathbf{t}_1 = 0$. The second orthogonal vector may be obtained by

$$\mathbf{t}_2 = \frac{\partial \kappa_i}{\partial \mathbf{x}_u} \times \mathbf{t}_1 \tag{59}$$

The vectors $\partial\kappa_i\partial\mathbf{x}_u, \mathbf{t}_1$, and $\mathbf{t}_2$ are by definition linearly independent and can be formed into an invertible matrix as follows

$$\mathbf{D}_i = \begin{bmatrix} \frac{\partial \kappa_i}{\partial \mathbf{x}_u} \\ \mathbf{t}_1 \\ \mathbf{t}_2 \end{bmatrix} \tag{60}$$

and Eqn. (58) may be written as

$$\delta\mathbf{x}_u = \mathbf{D}_i^{-1} \begin{bmatrix} \frac{\partial \kappa_i}{\partial \mathbf{x}_d} \\ \mathbf{0} \\ \mathbf{0} \end{bmatrix} \delta\mathbf{x}_d \tag{61}$$

Defining,a

$$\mathbf{N}_i = \mathbf{D}_i^{-1}\frac{\partial \kappa_i}{\partial \mathbf{x}_d} \tag{62}$$

and following the same statistical analysis shown in [27], it can be written that

$$\mathbf{P}_{i,\mathbf{x}_u} = \mathbf{N}_i\mathbf{P}_{\mathbf{x}_d}\mathbf{N}_i^T \tag{63}$$

Note that while Eqn. (63) is not explicitly a function of the observer position and timing errors and uncertainties, it is a function of the covariance on the position estimate which already accounts for the observer position and timing error. As shown in [27], the probability that a given state lies inside the i^{th} admissible region is now defined by a continuous function

$$\mathbb{P}(\mathbf{x}_u \in \mathcal{AR}_i) = \frac{1}{2}\left[1 - \text{erf}\left(\frac{\|\mathbf{x}_\text{u} - \mathbf{x}_{\text{u},\perp,\mathcal{AR}_\text{i}}\|}{\sqrt{2\text{tr}\mathbf{P}_{\text{i},\mathbf{x}_\text{u}}}}\right)\right] \tag{64}$$

where $\mathbf{x}_{u,\perp,\mathcal{R}_i}$ is the nearest point on the surface defined by Eqn. (54) orthogonal to $\mathbf{x}_u$. Unlike Eqn. (55), Eqn. (64) gives a continuous, smooth boundary at the edge of the admissible region. Assuming that each of the constraints are independent, the total probability that a point $\mathbf{x}_u$ lies inside of $\mathcal{R}$ is given by

$$\mathbb{P}(\mathbf{x}_u \in \mathcal{R}) = \prod_{i=1}^{c} \mathbb{P}(\mathbf{x}_u \in \mathcal{R}_i) \tag{65}$$

Eqn. (64) can be quantified for both constraints in this paper. Applying Eqn. (64) to Eqn. (31) define,

$$\|\mathbf{x}_u - \mathbf{x}_{u,\perp,\mathcal{R}_i}\| = \|\mathbf{x}_u\| - \mu\frac{2}{\mathbf{x}_d} \tag{66}$$

since the constraint surface is a sphere. The periapse radius constraint may be considered as essentially concentric spheres defined by a radius of $v_1 = +\sqrt{l_1}$ and $v_2 = +\sqrt{l_2}$ if l_1 and l_2 are real and positive for a given value of γ. The periapse radius constraint may be considered as the superposition of a sphere and hyperbolic body of revolution. In general, the quantity $\|\mathbf{x}_u - \mathbf{x}_{u,\perp,\mathcal{R}_2}\|$ can then be given by,

$$\|\mathbf{x}_u - \mathbf{x}_{u,\perp,\mathcal{R}_2}\| = \min(\|\mathbf{x}_\mathrm{u}\| - \mathrm{v}_1, \|\mathbf{x}_\mathrm{u}\| - \mathrm{v}_2\|) \tag{67}$$

Thus given any estimate $\mathbf{x}_d$ and a corresponding velocity $\mathbf{x}_u$, the probability that $\mathbf{x}_u$ is in the admissible region can be determined analytically as

$$\mathbb{P}(\mathbf{x}_u \in \mathcal{R}) = \frac{1}{4}\left[1 - \mathrm{erf}\left(\frac{\|\mathbf{x}_\mathrm{u}\| - \mu\frac{2}{\mathbf{x}_\mathrm{d}}}{\sqrt{2\mathrm{tr}\mathbf{P}_{1,\mathbf{x}_\mathrm{u}}}}\right)\right]\left[1 - \mathrm{erf}\left(\frac{\min(\|\mathbf{x}_\mathrm{u}\| - \mathrm{v}_1, \|\mathbf{x}_\mathrm{u}\| - \mathrm{v}_2\|)}{\sqrt{2\mathrm{tr}\mathbf{P}_{2,\mathbf{x}_\mathrm{u}}}}\right)\right] \tag{68}$$

SIMULATION

The purpose of this section is to demonstrate how an admissible region can be applied to the TDoA problem for space object initial orbit determination. The first subsection shows the importance of the observer location in the accuracy of the TDoA position estimate by showing the DOP for different observer configurations. The second subsection shows how an estimation scheme may be initiated from a set of TDoA measurements.

Observer Placement

Eqn. (22) is very sensitive to the placement of the observers. The DOP is effectively a measure of how accurate an estimate in a given region can be give the configuration of the observer stations. To demonstrate this, 3 configurations will be used to demonstrate the effect on DOP. The latitude and longitude of each observer site for each configuration is shown in Table 1. The purpose of choosing these observer configurations is to demonstrate the baseline between observing stations required for good TDoA DOP.

In general, the TDoA DOP is very similar to DOP as seen in GPS measurements. A geometric configuration with GPS satellites dispersed across the sky provides a much lower DOP, and thus higher accuracy, measurement that if the GPS satellites are clustered. Likewise, the TDoA DOP is centered around the dispersion of the observers. Figures 3-5 show how DOP changes with the

	North America	Southeast	Atlanta
Site 1	(33.7774, -84.3989)	(34.9253, -80.9841)	(33.7774, -84.3989)
Site 2	(34.1374, -118.1256)	(33.7899, -84.4025)	(33.7671, -84.2951)
Site 3	(42.3608, -71.0928)	(30.2798, -81.4849)	(33.7951, -84.3214)
Site 4	(30.2852, -97.7348)	(36.2180, -86.7638)	(33.7454, -84.4120)

Table 1: The observer locations for the DOP analysis

position of the source of the signal. For these calculations, DOP is only computed if a particular source position has line of sight to each observer.

The geometric line of sight restriction can be seen in Figure 3b where the shape of the iso-surface dips back toward the Earth near the centerline of the observer locations. This contrasts directly with the plots in Figure 4, where the iso-surface of coverage is a smooth dome shape over the region. It is worth mentioning that while the North America and Southeast observer cases perform reasonably well regarding DOP, the Atlanta based observers perform very poorly due to the geometry of the observers. At these levels of DOP, the uncertainty in the measurements is on the same order of magnitude as radius of the Earth. With such poor DOP, a TDoA system based on a tight observer configuration, such as a city, would be unable to provide any useful information on the position of the source object.

Position Estimate Using TDoA

Admissible region approaches can be used to initiate filters by sampling from the admissible region itself. The purpose of this section is to show the geometry of the admissible region for the TDoA problem and demonstrate the initialization of a particle filter from the admissible region. Since the lowest DOP is achieved with the North America configuration, it is used as the observer positions for this section. For the purposes of this section, the true object state is given as

$$\mathbf{x}_{d,\text{true}} = \begin{bmatrix} -0.9121 & 0.3707 & 0.6046 \end{bmatrix} \text{ DU} \tag{69}$$

$$\mathbf{v}_{\text{true}} = \begin{bmatrix} -0.5571 & -0.5820 & -0.4253 \end{bmatrix} \text{ DU/TU} \tag{70}$$

The standard deviations on the observer position knowledge and timing error are taken to be

$$\sigma_{r_s} = 1\text{m} \tag{71}$$

$$\sigma_t = 5 \times 10^{-9}\text{s} \tag{72}$$

With these covariances defined, a position estimate for the source object by directly solving Eqns. (4)-(7).

$$\mathbf{x}_d = \begin{bmatrix} -0.9121 & 0.3708 & 0.6047 \end{bmatrix} \text{ DU} \tag{73}$$

The covariance of the $\mathbf{z}$ vector is then given by

$$\mathbf{P}_\mathbf{z} = \begin{bmatrix} \sigma_{r_s}^2 \mathbf{I}_{(12\times 12)} & \mathbf{0} \\ \mathbf{0} & \sigma_t^2 \mathbf{I}_{(4\times 4)} \end{bmatrix} \tag{74}$$

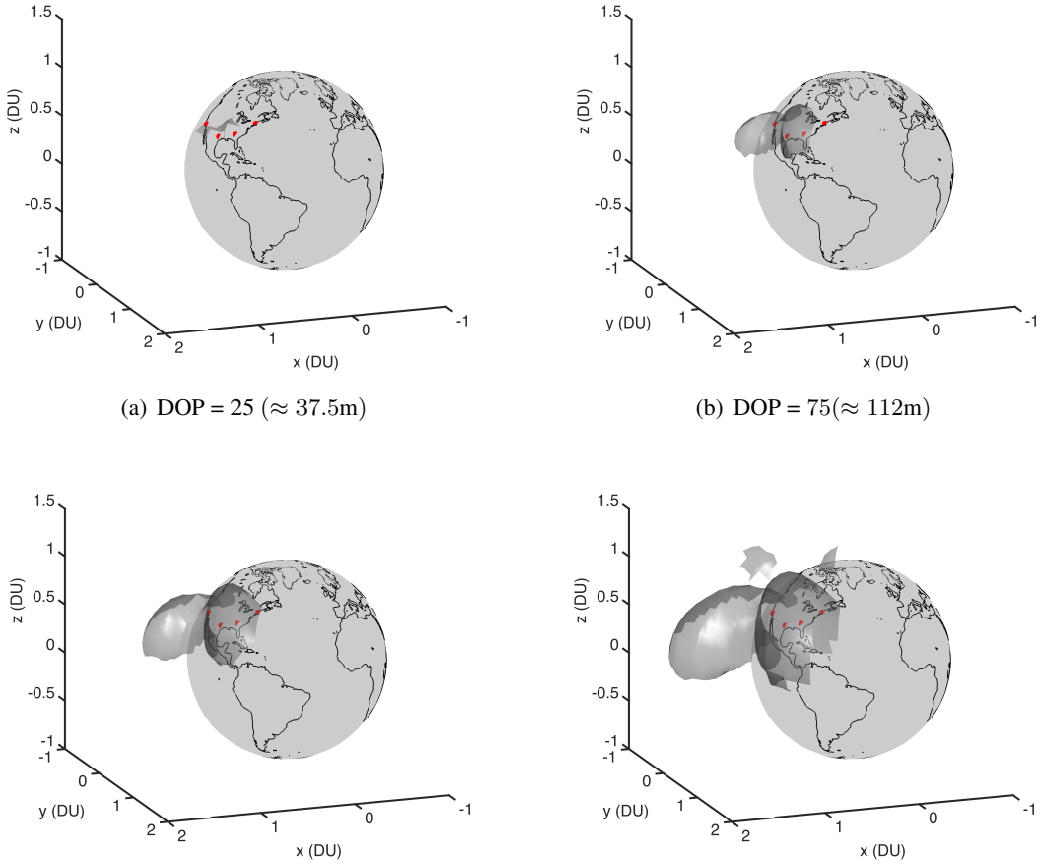

(a) DOP = 25 ($\approx$ 37.5m)

(b) DOP = 75($\approx$ 112m)

(c) DOP = 150($\approx$ 225m)

(d) DOP = 300($\approx$ 450m)

Figure 3: Iso-surfaces of DOP for the North America observer case

And the covariance on the estimate shown is given by evaluating Eqn. (20). Taking the diagonal elements of $\mathbf{P}_{\mathbf{x}_d}$ gives the covariances on the estimate of the object position and the time delay in the system.

$$\sigma_{\mathbf{x}_{d,x}} = 0.1657 \times 10^{-5} \text{ DU} = 10.571\text{m} \tag{75}$$

$$\sigma_{\mathbf{x}_{d,y}} = 0.7645 \times 10^{-5} \text{ DU} = 48.762\text{m} \tag{76}$$

$$\sigma_{\mathbf{x}_{d,z}} = 0.1213 \times 10^{-5} \text{ DU} = 7.734\text{m} \tag{77}$$

$$\sigma_{c\tau} = 0.7506 \times 10^{-5} \text{ DU} = 47.870\text{m} \tag{78}$$

The DOP for this measurement is then given by evaluating Eqn. (22) giving,

$$D_P = 47.2717 \tag{79}$$

which is a unitless quantity.

Filter Initiation Using TDoA Admissible Regions

The estimate and covariance obtained only correspond to the position of the object, the admissible region must be applied to bound the velocities consistent with this object position in order to initiate

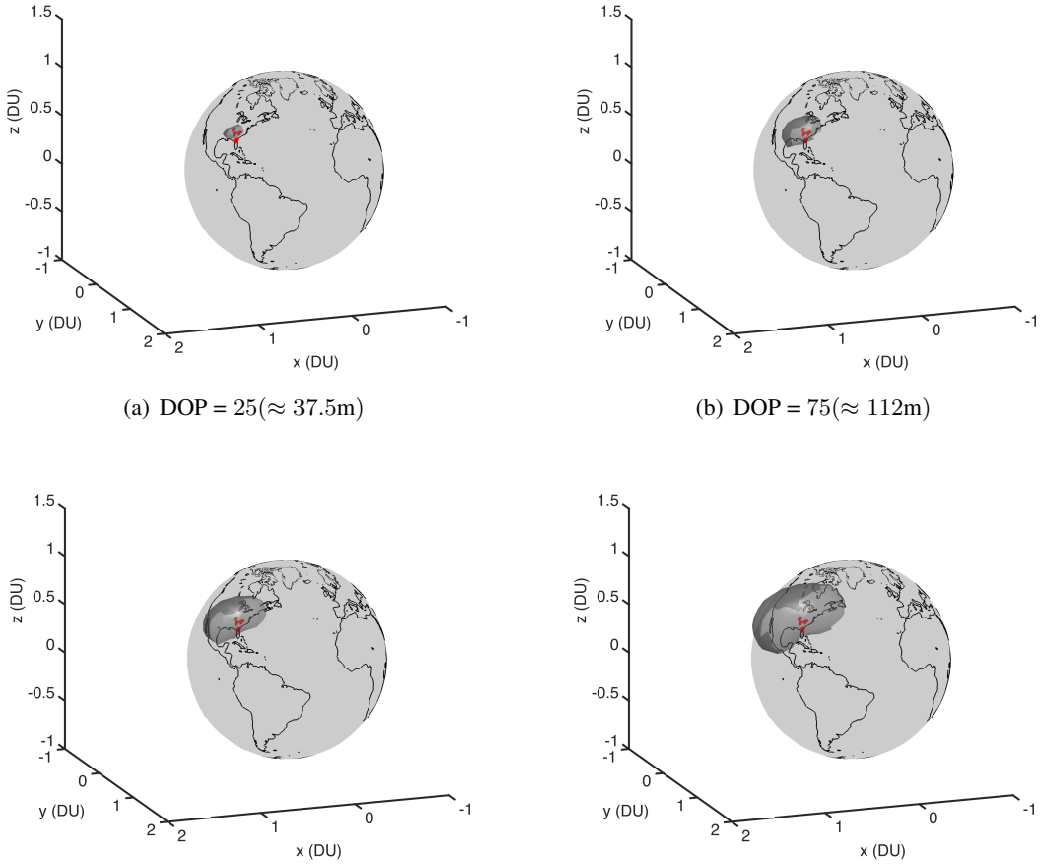

(a) DOP = $25(\approx 37.5\text{m})$ (b) DOP = $75(\approx 112\text{m})$

(c) DOP = $150(\approx 225\text{m})$ (d) DOP = $300(\approx 450\text{m})$

Figure 4: Iso-surfaces of DOP for the Southeast observers case

a filter. An overview of the procedure is shown in Figure 6. Following the outline, the admissible must now be constructed after the position estimate is made.

A joint admissible region is considered by generating the energy and periapse radius admissible regions individually and taking the piecewise product to be the joint admissible region. The estimate covariance is included in the admissible region formulation to account for the errors in timing and position accuracy of the observers through their impact on the estimate. These uncertainties have a considerable effect on the admissible region and the boundaries of the admissible region are thus expanded, accounting for vastly more states than if uncertainties are neglected. To demonstrate this, a joint admissible region with and without uncertainties is generated and the resulting sampled points are shown in Figures 7 and 8. As can be seen, there is a much smaller set of points spanning the state space when no uncertainty is considered. The covariance on the position estimate conveys how accurate the estimate is and it is expected that with less accuracy, more possible undetermined state solutions must be considered and this is reflected in Figures 7 and 8. The sampled points in Figure 8 will be used to initiate a particle filter for to get a velocity estimate.

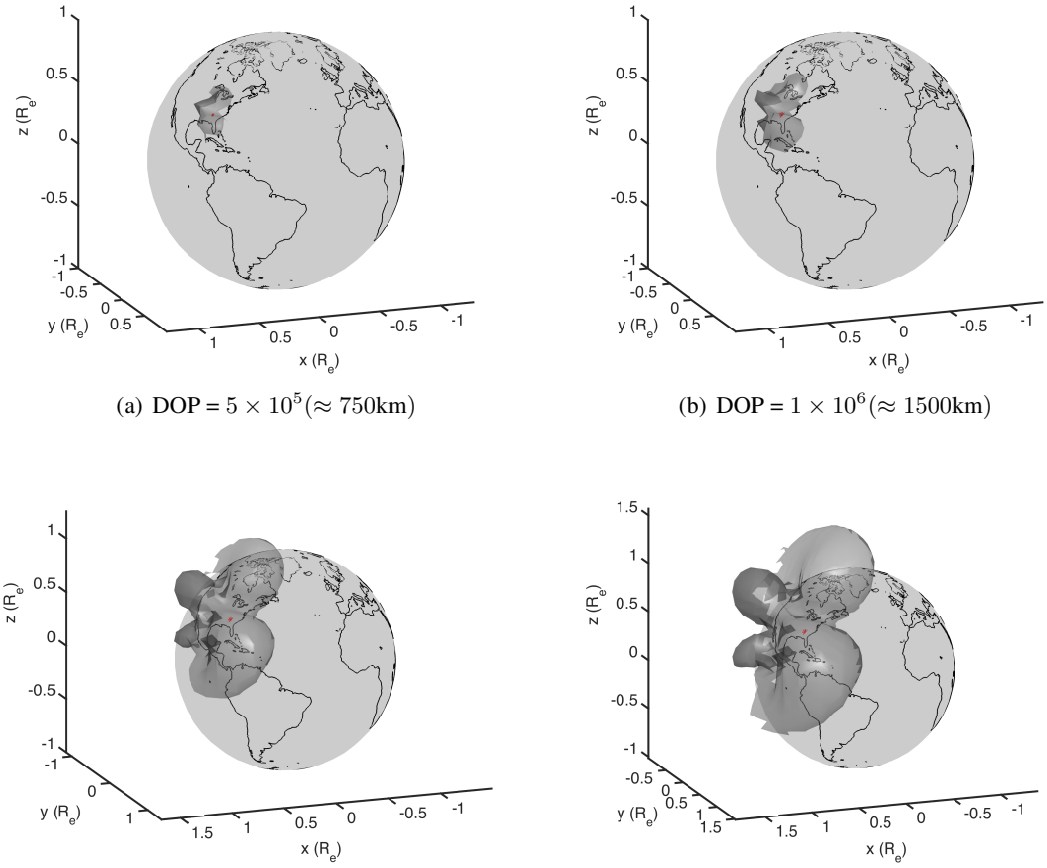

(a) DOP = $5 \times 10^5 (\approx 750\text{km})$

(b) DOP = $1 \times 10^6 (\approx 1500\text{km})$

(c) DOP = $5 \times 10^6 (\approx 7500\text{km})$

(d) DOP = $1 \times 10^7 (\approx 15000\text{km})$

Figure 5: Iso-surfaces of DOP for the Atlanta based observers case

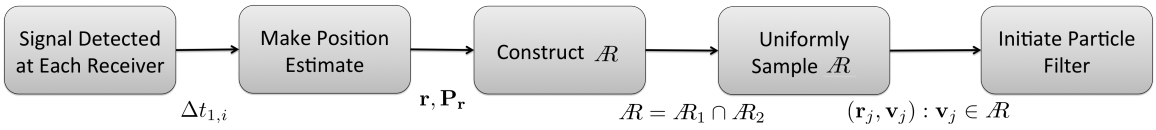

Figure 6: Outline of the filter initiation process using TDoA measurements

The particle filter used in this example will use the PDF defined by

$$f(\mathbf{x}_u) = \frac{\mathbb{P}(\mathbf{x}_u \in \mathcal{R})}{\int_{\mathcal{R}} \mathrm{d}\mathbf{x}_\mathrm{u}} \tag{80}$$

as the initial weighting for each of the points sampled from the admissible region. The particle filter assumes a new measurement is available 2 hours after the first measurement and the resulting distribution of velocity states are shown in the Figures below. Figure 9 shows the new distribution of particles after the new measurement is made. For a point of comparison, the same analysis is performed on the set of points shown in Figure 7 where no uncertainty is included. Figure 11 show the results from the particle filter initiated on an admissible region for TDoA measurements both with and without measurement uncertainties taken into account. Likewise, 12 shows the resulting

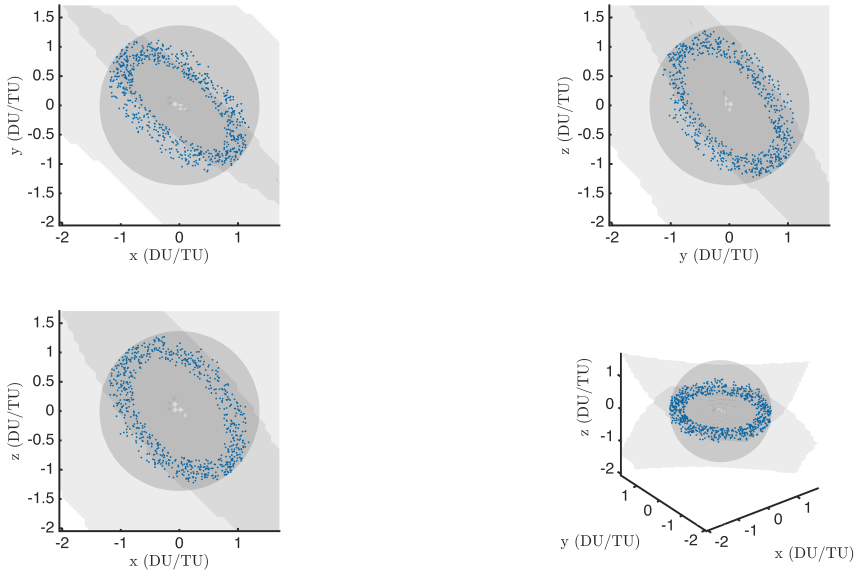

Figure 7: Sampled points from the joint admissible region without considering the covariance on the position estimate. The different views show the geometry of the admissible region constraints.

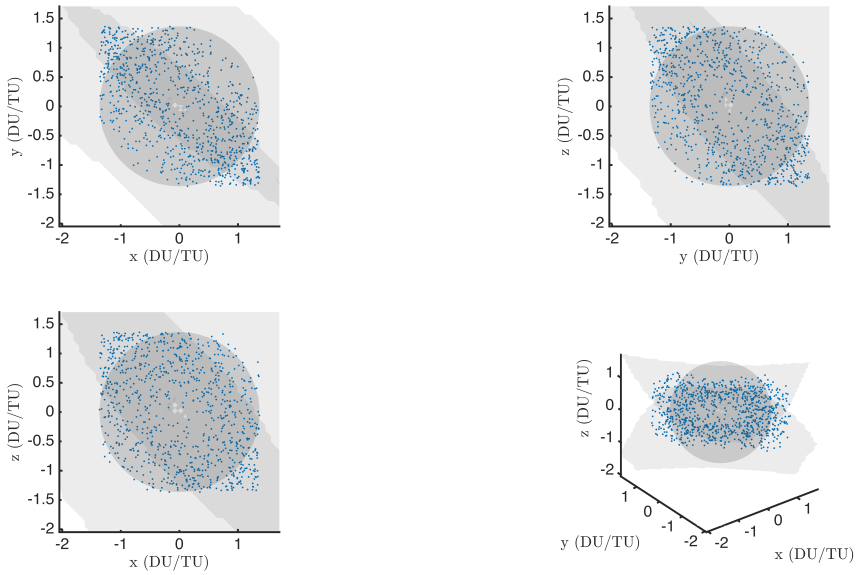

Figure 8: Sampled points from the joint admissible region considering the covariance on the position estimate. As can be seen, the uncertainty relaxes the constraint boundary and more points are included closer to the center of the sphere as well as outside the hyperbola bounds.

distribution of the position after the measurement is ingested for both the uncertainty and no uncertainty cases. This figure serves to show a representation of how a particle filter initiated on a set of TDoA measurements would behave. In this particular example, it appears that the inclusion of

uncertainty in the generation of the admissible region yields a better distribution of particles near the true source object velocity.

CONCLUSIONS AND FUTURE WORK

This paper shows how the concept of admissible regions for initial orbit determination can be applied to a set of time differential of arrival (TDoA) measurements. The effects of uncertainty on the TDoA position estimate and the impact of dilution of precision (DOP) of the measurement are shown. The underdetermined and determined states for TDoA measurements are identified as the velocity and position of the observer respectively. Energy and periapse radius are considered as constraint hypotheses to constraint the admissible region. An analytical approach is then derived which enables a direct solution for the probability that a given velocity state is in the admissible region. An example TDoA observation simulation is shown, comparing DOP for different observer configurations. From the best observer configuration an admissible region is constructed and sampled to initialize a particle filter.

The results shown in this paper focus on ground based observers for TDoA using signals of opportunity. Future work will include an application of TDoA to space based observers and the design of observer placement for space based TDoA measurements. The TDoA solution as proposed in [13], assumes that the observers all share a common focus. Space based observers will not satisfy this criteria and an alternative solution approach must be employed. In this paper, the signals were considered to be received at the observer with some prescribed uncertainty in timing error and position knowledge. A full treatment of the signal processing, matched filtering, and signal arrival difference is planned for future work. A comparison will also be made between the admissible regions of TDoA measurements and those of radar measurements.

ACKNOWLEDGEMENTS

This material is based upon work supported by the National Science Foundation Graduate Research Fellowship under Grant No. DGE-1148903.

REFERENCES

[1] R. Bucher and D. Misra, "A Synthesizable VHDL Model of the Exact Solution for Three-dimensional Hyperbolic Positioning System," *VLSI Design*, Vol. 15, No. 2, 2002, pp. 507–520.

[2] R. Kaune, C. Steffes, S. Rau, W. Konle, and J. Pagel, "Wide area multilateration using ADS-B transponder signals," *Information Fusion (FUSION), 2012 15th International Conference on*, IEEE, 2012, pp. 727–734.

[3] J. Stefanski, "Asynchronous wide area multilateration system," *Aerospace Science and Technology*, Vol. 36, No. 0, 2014, pp. 94 – 102, http://dx.doi.org/10.1016/j.ast.2014.03.016.

[4] T. A. Webb, P. D. Groves, P. A. Cross, R. J. Mason, and J. H. Harrison, "A new differential positioning method using modulation correlation of signals of opportunity," 2010.

[5] P. R. Escobal, "3-D multilateration: A precision geodetic measurement system," *Technical Memorandum 33-605, Jet Propulsion Laboratory*, March 1973.

[6] P. R. Escobal, K. M. Ong, and O. V. Roos, "Range difference multilateration for obtaining precision geodetic and trajectory measurements," *Acta Astronautica*, Vol. 2, 1975, pp. 481–495.

[7] K. Ho and Y. Chan, "Solution and performance analysis of geolocation by TDOA," *Aerospace and Electronic Systems, IEEE Transactions on*, Vol. 29, No. 4, 1993, pp. 1311–1322.

[8] K. Ho and Y. Chan, "Geolocation of a known altitude object from TDOA and FDOA measurements," *Aerospace and Electronic Systems, IEEE Transactions on*, Vol. 33, July 1997, pp. 770–783, 10.1109/7.599239.

[9] N. Okello and D. Musicki, "Emitter Geolocation with Two UAVs," *Information, Decision and Control, 2007. IDC '07*, Feb 2007, pp. 254–259, 10.1109/IDC.2007.374559.

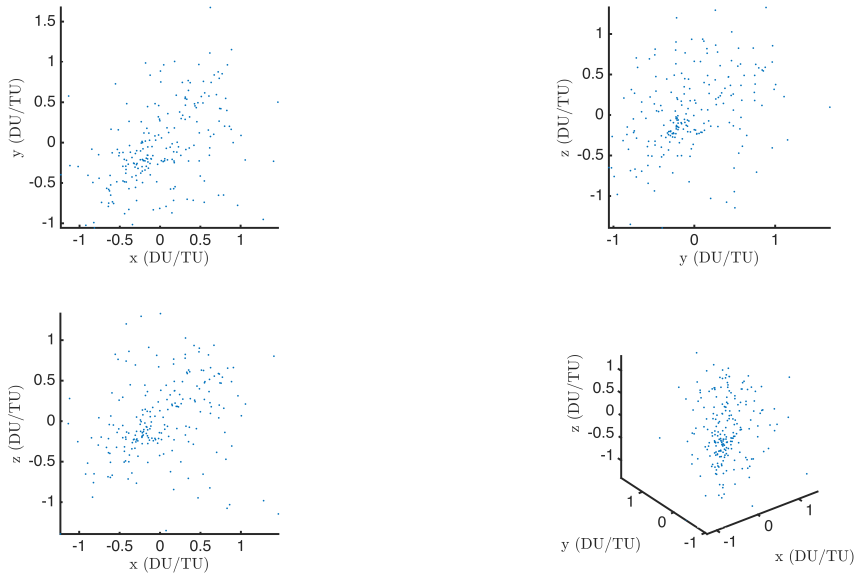

Figure 9: The resulting distribution of particle velocities after the second measurement is ingested.

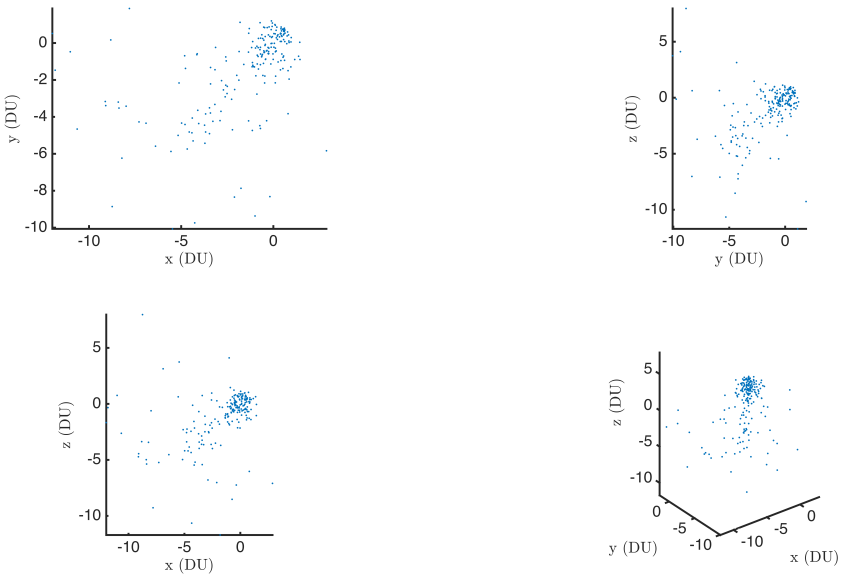

Figure 10: The resulting distribution of particle positions after the second measurement is ingested.

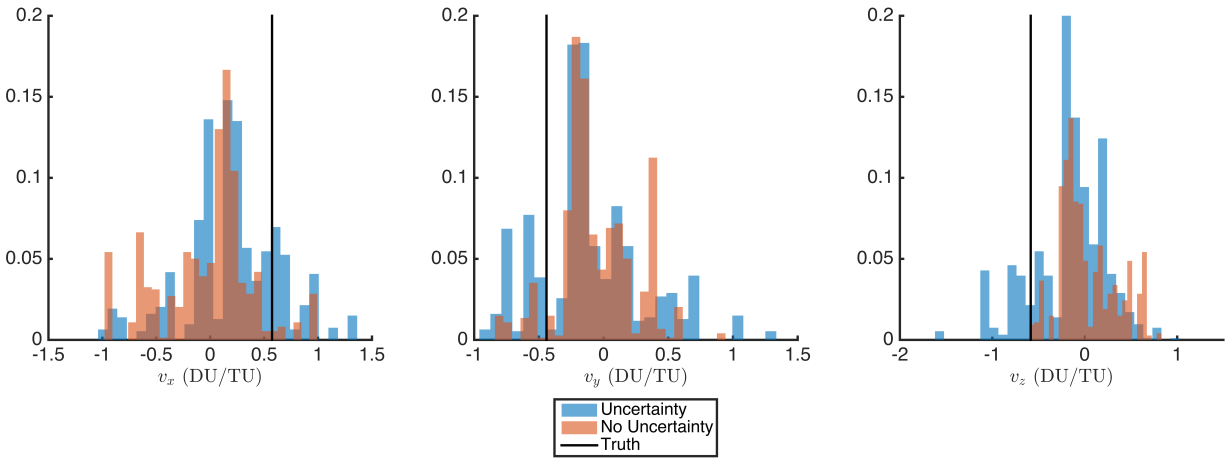

Figure 11: Results comparing the initialization of a particle filter with and $\mathcal{AR}$ with and without considering uncertainties.

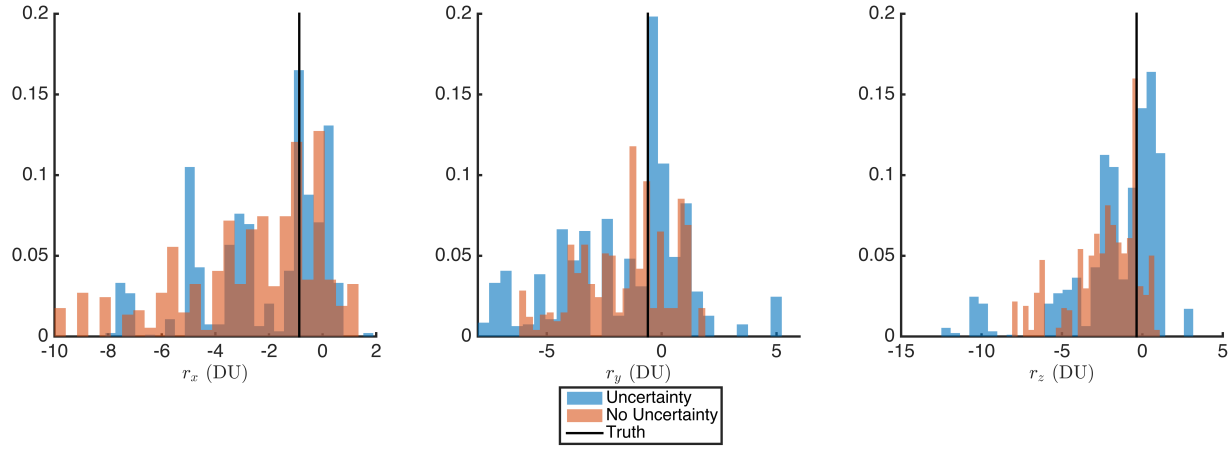

Figure 12: The resulting distribution particle positions compared with the true object position.

[10] F. Fletcher, B. Ristic, and D. Musicki, "Recursive estimation of emitter location using TDOA measurements from two UAVs," *Information Fusion, 2007 10th International Conference on*, IEEE, 2007, pp. 1–8.

[11] D. Musicki and W. Koch, "Geolocation using TDOA and FDOA measurements," *Information Fusion, 2008 11th International Conference on*, IEEE, 2008, pp. 1–8.

[12] S. Stein, "Algorithms for ambiguity function processing," *Acoustics, Speech and Signal Processing, IEEE Transactions on*, Vol. 29, Jun 1981, pp. 588–599, 10.1109/TASSP.1981.1163621.

[13] Y. Chan and K. Ho, "A simple and efficient estimator for hyperbolic location," *Signal Processing, IEEE Transactions on*, Vol. 42, Aug 1994, pp. 1905–1915, 10.1109/78.301830.

[14] D. Musicki and R. J. Evans, "Measurement Gaussian sum mixture target tracking," *Information Fusion, 2006 9th International Conference on*, IEEE, 2006, pp. 1–8.

[15] A. J. Sinclair, T. A. Lovell, and J. Darling, "RF localization solution using heterogeneous TDOA," *Aerospace Conference, 2015 IEEE*, IEEE, 2015, pp. 1–7.

[16] V. Sark and E. Grass, "Modified equivalent time sampling for improving precision of time-of-flight based localization," *Personal Indoor and Mobile Radio Communications (PIMRC), 2013 IEEE 24th International Symposium on*, Sept 2013, pp. 370–374, 10.1109/PIMRC.2013.6666163.

[17] D. Geiger, "High Resolution Time Difference of Arrival Using Timestamps for Localization in 802.11b/g Wireless Networks," *Wireless Communications and Networking Conference (WCNC), 2010 IEEE*, April 2010, pp. 1–6, 10.1109/WCNC.2010.5506558.

[18] R. Gerdes, T. Daniels, M. Mina, and S. Russell, "Device Identification via Analog Signal Fingerprinting: A Matched Filter Approach," *Network and Distributed System Security Symposium*, 2006.

[19] M. Robinson and R. Ghrist, "Topological Localization Via Signals of Opportunity," *Signal Processing, IEEE Transactions on*, Vol. 60, May 2012, pp. 2362–2373, 10.1109/TSP.2012.2187518.

[20] J. Bard and F. Ham, "Time difference of arrival dilution of precision and applications," *Signal Processing, IEEE Transactions on*, Vol. 47, Feb 1999, pp. 521–523, 10.1109/78.740135.

[21] J. Do, M. Rabinowitz, P. Enge, *et al.*, "Performance of TOA and TDOA in a non-homogeneous transmitter network combining GPS and terrestrial signals," *Proc. ION National Technical Meeting*, 2006, pp. 642–649.

[22] K. DeMars, M. Jah, and P. Schumacher, "Initial Orbit Determination using Short-Arc Angle and Angle Rate Data," *Aerospace and Electronic Systems, IEEE Transactions on*, Vol. 48, No. 3, 2012, pp. 2628–2637, doi:10.1109/TAES.2012.6237613.

[23] J. M. Maruskin, D. J. Scheeres, and K. T. Alfriend, "Correlation of Optical Observations of Objects in Earth Orbit," *Journal of Guidance, Control, and Dynamics*, Vol. 32, No. 1, 2009, pp. 194–209, doi:10.2514/1.36398.

[24] K. Fujimoto, J. Maruskin, and D. Scheeres, "Circular and zero-inclination solutions for optical observations of Earth-orbiting objects," *Celestial Mechanics and Dynamical Astronomy*, Vol. 106, No. 2, 2010, pp. 157–182, doi:10.1007/s10569-009-9245-y.

[25] A. Milani, G. F. Gronchi, M. d. Vitturi, and Z. Knežević, "Orbit determination with very short arcs. I admissible regions," *Celestial Mechanics and Dynamical Astronomy*, Vol. 90, No. 1-2, 2004, pp. 57–85, doi:10.1007/s10569-004-6593-5.

[26] A. Milani, G. F. Gronchi, Z. Knežević, M. E. Sansaturio, and O. Arratia, "Orbit determination with very short arcs: II. Identifications," *Icarus*, Vol. 179, No. 2, 2005, pp. 350 – 374, doi:10.1016/j.icarus.2005.07.004.

[27] J. L. Worthy and M. J. Holzinger, "Incorporating Uncertainty in Admissible Regions for Uncorrelated Detections," *Journal of Guidance, Control, and Dynamics*, 2015/04/09 2015, pp. 1–17, 10.2514/1.G000890.

[28] D. Farnocchia, G. Tommei, A. Milani, and A. Rossi, "Innovative methods of correlation and orbit determination for space debris," *Celestial Mechanics and Dynamical Astronomy*, Vol. 107, No. 1-2, 2010, pp. 169–185.